SUPPLEMENTARY INFORMATION
https://doi.org/10.1038/s41565-018-0245-5

In the format provided by the authors and unedited.

Directional lasing in resonant semiconductor nanoantenna arrays

Son Tung Ha[1,2,5], Yuan Hsing Fu[1,3,5], Naresh Kumar Emani[1,4,5], Zhenying Pan[1,2], Reuben M. Bakker[1,2], Ramón Paniagua-Domínguez[1,2] and Arseniy I. Kuznetsov[1,2]*

[1]Data Storage Institute, Agency for Science, Technology and Research, Singapore, Singapore. [2]Present address: Institute of Materials Research and Engineering, Agency for Science, Technology and Research, Singapore, Singapore. [3]Present address: Institute of Microelectronics, Agency for Science, Technology and Research, Singapore, Singapore. [4]Present address: Indian Institute of Technology, Hyderabad, India. [5]These authors contributed equally: Son Tung Ha, Yuan Hsing Fu, Naresh Kumar Emani. *e-mail: arseniy_kuznetsov@imre.a-star.edu.sg

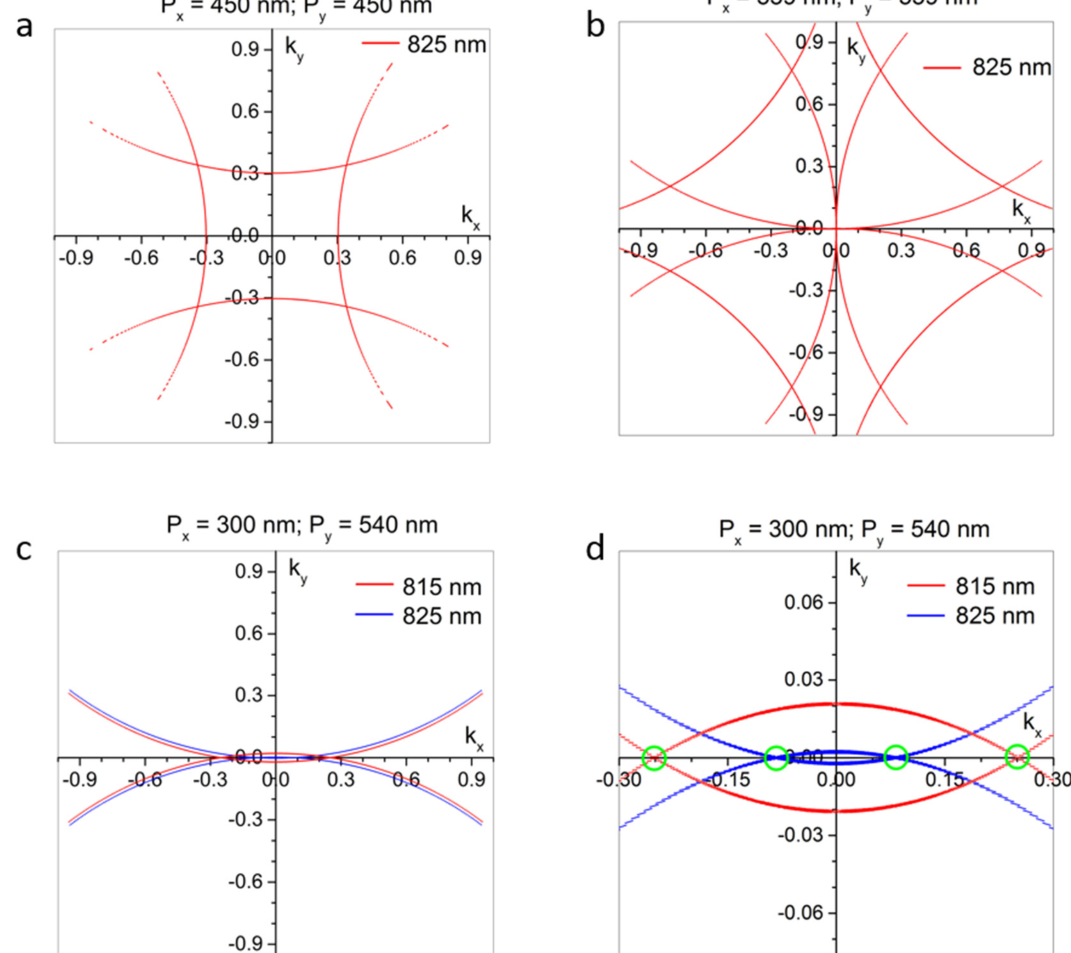

Supplementary Fig.1. Theoretical calculation of the emission bands for a 2D GaAs array with different periods and wavelengths based on reciprocity.[1] a, For P_x = 450 nm, P_y = 450 nm and 825 nm wavelength (sub diffractive at normal incidence/emission). b, For P_x = 539 nm, P_y = 539 nm and 825 nm wavelength (supporting diffractive modes at normal incidence/emission). c, For P_x = 300 nm, P_y = 540 nm and 815 nm (red) and 825 nm (blue) wavelengths (below diffraction in x-axis and slightly above diffraction in y-axis). d, Zoom-in emission band in c, showing the emission cross-point at k_x at small angle for 825 nm emission and larger angle for 815 nm emission.

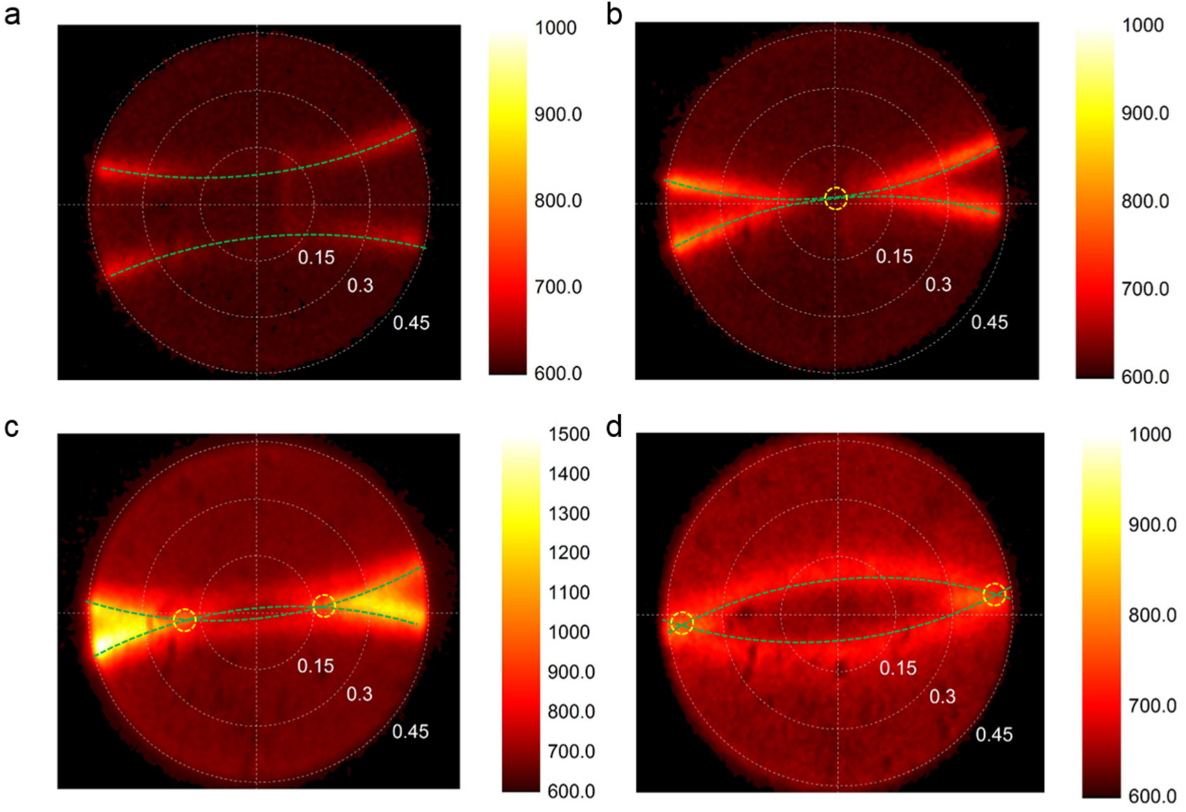

Supplementary Fig.2. Experimental back focal plane emission patterns. a, P_y = 530 nm (subdiffractive at normal incidence/emission). b, P_y = 540 nm (supporting diffraction at normal incidence/emission). c, P_y = 550 nm – (slightly above diffraction at normal incidence/emission). d, P_y = 590 nm – (above diffraction at normal incidence/emission). All results are for emission wavelength around 830 nm. In all cases the period along the x-axis, P_x, is fixed at 300 nm. The signals were collected using long working distance (WD) objective (50X, WD = 17 mm) with numerical aperture NA = 0.45 resulting in a maximum collection angle of ~ 28 degree.

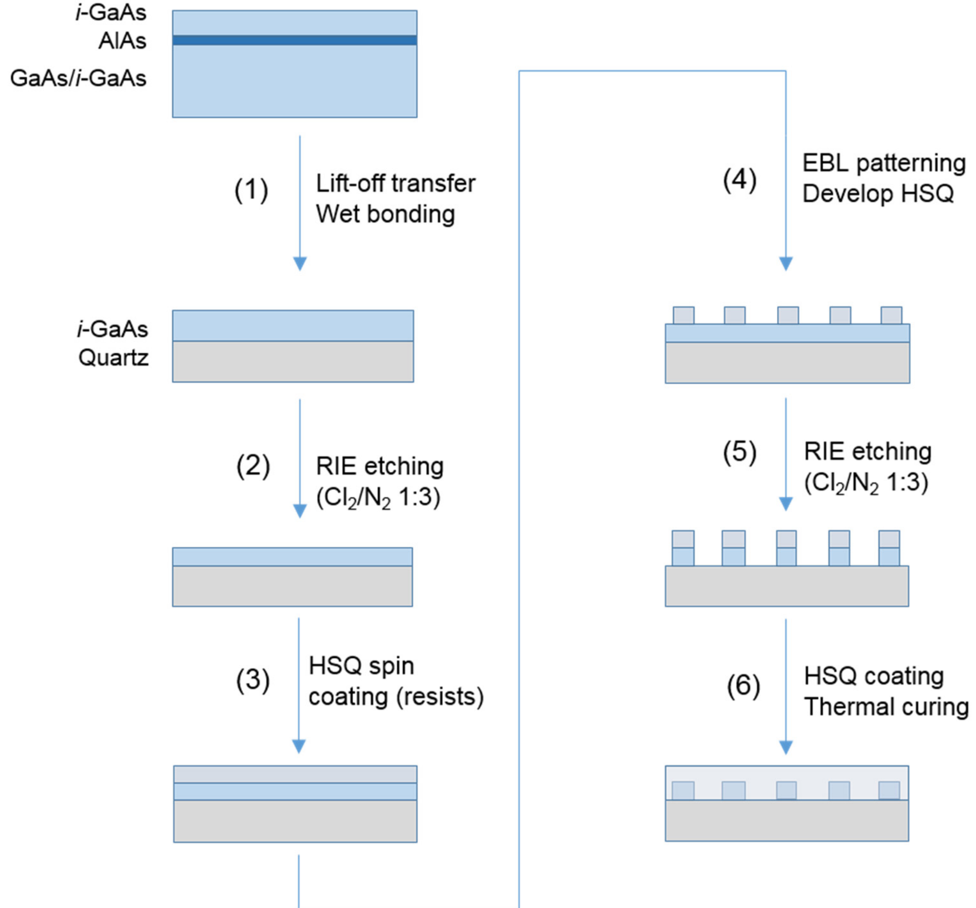

Supplementary Fig.3. Fabrication steps for GaAs nanopillar arrays. (1) The fabrication starts with a *i*-GaAs/AlAs/*i*-GaAs wafer purchased from Semiconductor Wafer, Inc (Taiwan). The bottom GaAs (substrate) layer consists of 625 μm undoped <100> GaAs. The middle layer is AlAs with a thickness of 100 nm. The top layer is *i*-GaAs with a thickness of 500 nm. To obtain the GaAs film we follow the epitaxial lift-off process described by Yablonovitch *et al.*[2,3] In the process black wax (*i.e.,* Apiezon W) is applied on the top *i*-GaAs layer and thermally annealed at 90°C for about 30-60 mins to realize a slightly domed surface. The sample is then placed in dilute hydrofluoric acid (HF) solution (~5 wt. % in H_2O) overnight to selectively remove the AlAs layer. The top *i*-GaAs layer along with the wax detaches from the wafer and floats in the aqueous etchant solution. The *i*-GaAs film is then gently placed on a fused silica substrate (quartz) and the interfacial water layer is left to dry out. When the water is evaporated the GaAs film will stick to underlying quartz due to Van der Waals forces. Finally, the wax layer is removed by placing the sample in Dichloromethane (other polar solvents like Xylene and Trichloroethylene will work as well) and cleaned Acetone, IPA and H_2O. (2)

Inductively Coupled Reactive ion etching (ICP-RIE, Oxford Plasmapro) using Cl_2 chemistry is used to etch the initial thickness of *i*-GaAs (*i.e.,* 500 nm) to about 250 nm as in our design. The GaAs film thickness before and after etch was monitored using spectral reflectance measurements (Filmetrics F20). (3) A negative resist – Hydrogen silsesquioxane (HSQ, XR1541-6, Dow Corning) is coated directly onto *i*-GaAs at 5000 RPM for 90 seconds and baked on a hotplate at 140°C for 3 minutes. (4) Electron beam lithography is used to pattern the nanopillar array into HSQ. The HSQ film is then developed in 25% Tetramethyl Ammonium Hydroxide (TMAH) in H_2O. (5) ICP-RIE is used again to obtain GaAs pillar pattern using the patterned HSQ as the mask. (6) The GaAs arrays were covered in a thick layer of HSQ resist by repeated spin-coating and thermal curing steps. The curing process cross links and hardens the HSQ resist resulting in the formation of Spin On Glass with refractive index close to 1.5.

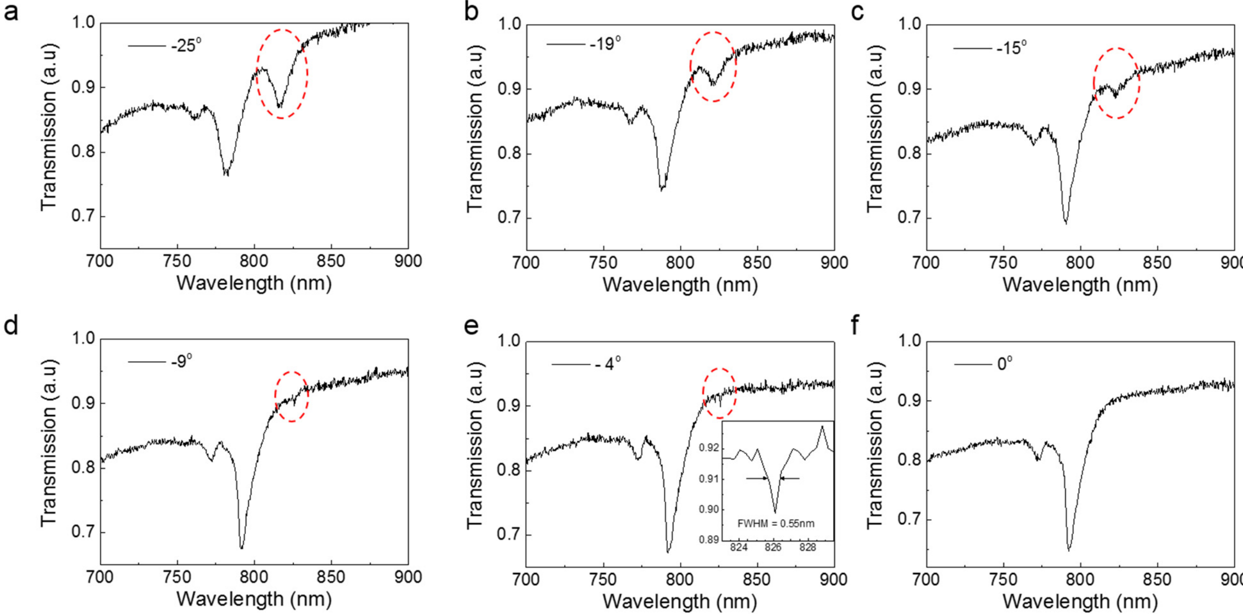

Supplementary Fig.4. Transmission spectra at different angles. Transmission data, as extracted from Figure 2b in the main text, for different angles: As can be seen, the resonance at ~ 825 nm vanishes at 0 degree while the other mode at ~ 790 nm is just red-shifted for decreasing angle of incidence.

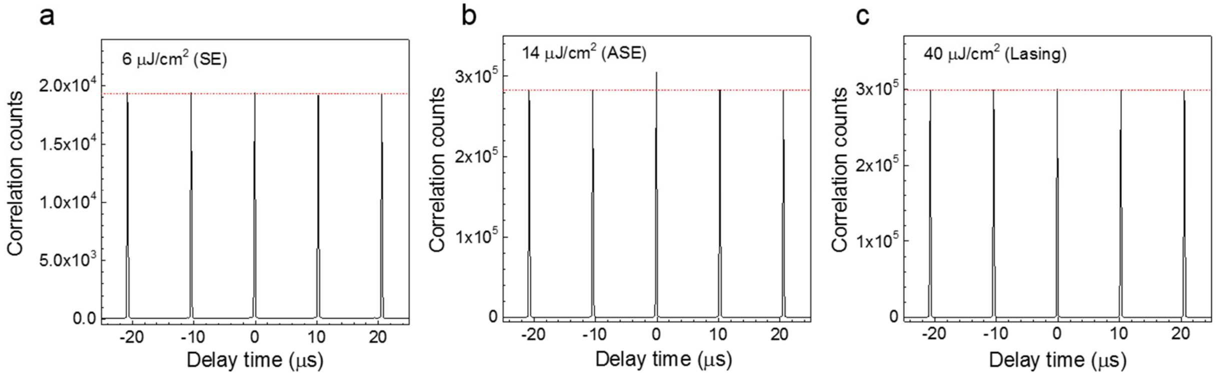

Supplementary Fig.5. Second-order photon correlation function measurement. To measure the second-order correlation function of the emitted light in our device, we routed the signal in our microscopic lasing measurement setup into a multimode fibre (Thorlabs GIF625, 62.5 µm core). The signal was then sent to a 50:50 optical fibre beamsplitter, and we measured the coincident clicks on the two low-jitter avalanche photodiodes (Micro Photon Devices, PDM series with a timing jitter of 35ps FWHM) at the output using a time-tagging device (qutools, QuTAU, timing resolution 81ps). The above figures show the measured histograms at different pumping fluences corresponding to (a) spontaneous emission (SE); (b) Amplified spontaneous emission (ASE); and (c) Lasing regime. The integrated intensity of correlation at zero time delay was then normalized to the average integrated intensity from the neighbouring pulses to calculate $g^2(0)$ for different pumping fluences, as shown in Figure 3b bottom panel.

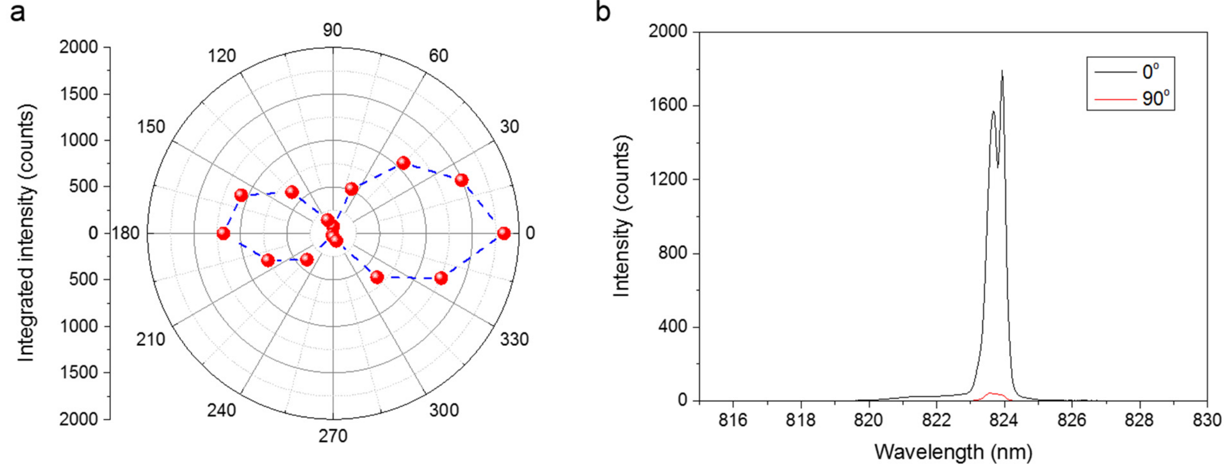

Supplementary Fig.6. Polarization dependence of the lasing. The lasing signal after the collection objective is passed through a polarizer with controlled polarization angle before being collected by the spectrometer. We defined 0° (180°) angle to correspond to direction along y axis of the array. a, Lasing intensity dependence on polarization angle showing maximum at 0 and 180° (along x axis), consistent with the vertical dipole orientation, from which the leaky resonance emerges, and the lasing directivity as discussed in Figure 3 in the main text. The asymmetry of the polarization dependence may come from variations in the signal collection and/or pumping laser power fluctuations. b, Lasing spectra for polarization at 0 and 90° showing at least 2 orders of magnitude difference in the intensity.

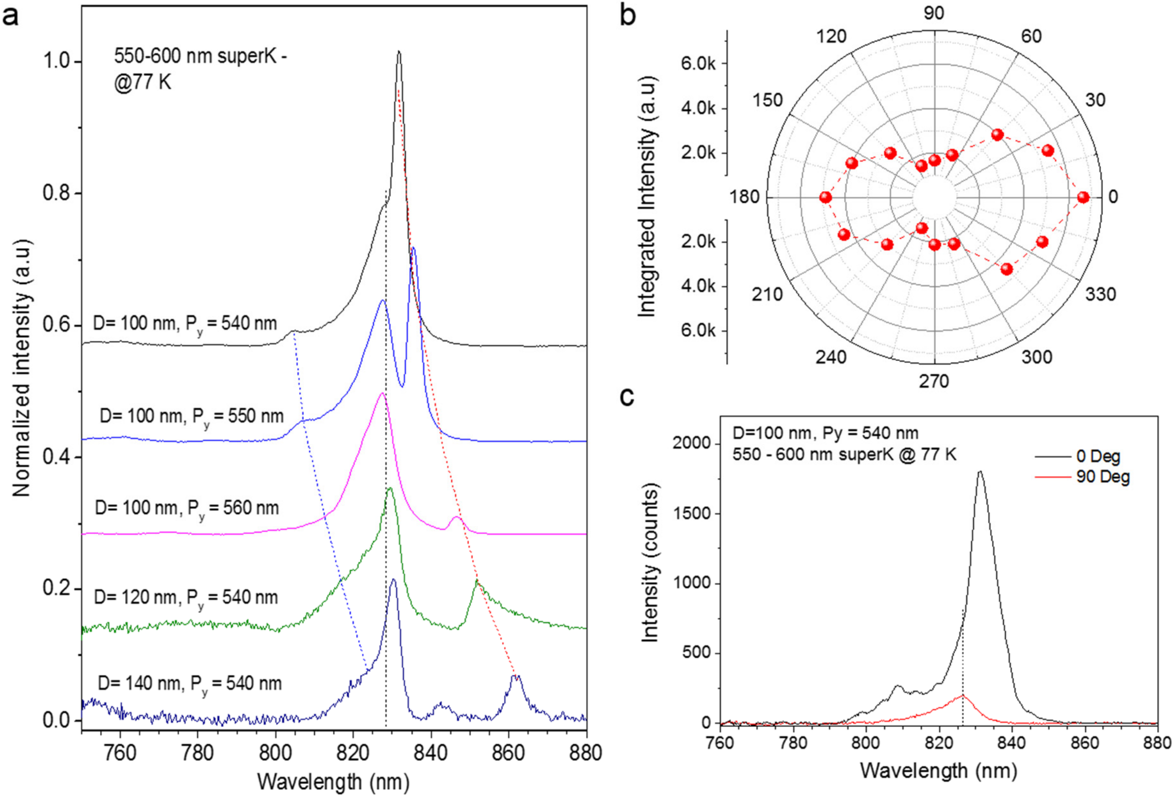

Supplementary Fig.7. Resonantly enhanced photoluminescence study. In this experiment we used a supercontinuum laser (superK, NKT) as a pumping source. The pumping wavelength range of 550- 600 nm was selected using a variable bandpass filter. This laser has 80 MHz repetition rate and a pulse duration of a few hundred picoseconds. This results in a much lower laser fluence compared to the femtosecond laser source used in lasing experiments. Nevertheless, resonantly enhanced photoluminescence peaks can be observed. **a,** Emission spectra measured for different GaAs nanopillar arrays with parameters labeled in the figure (D – diameter of the nanopillar; P_y – array period in y direction; P_x and height of the nanopillars were kept at 300nm and 250 nm, similar to the lasing array studied in the main text). They show a photoluminescence peak at around 828 nm and 2 sets of narrower peaks enhanced by the horizontal dipole resonance (shorter wavelength peak) and the vertical dipole resonance (longer wavelength peak) which is consistent with the angle resolved transmission measurement in Figure 2b in the main text. For the lasing array with D = 100nm and P_y = 540 nm the vertical dipole-enhanced peak is overlapped with the PL peak of GaAs (at 77K). This explains why the emission band for the lasing array vanishes near 0°, as shown in Figure 3d in the main text, as the photoluminescence is resonantly enhanced by vertical dipole

resonance, which does not emit in the vertical direction. **b** and **c,** polarization dependence of resonant enhanced photoluminescence showing similar behavior as the lasing emission shown in Figure S6.

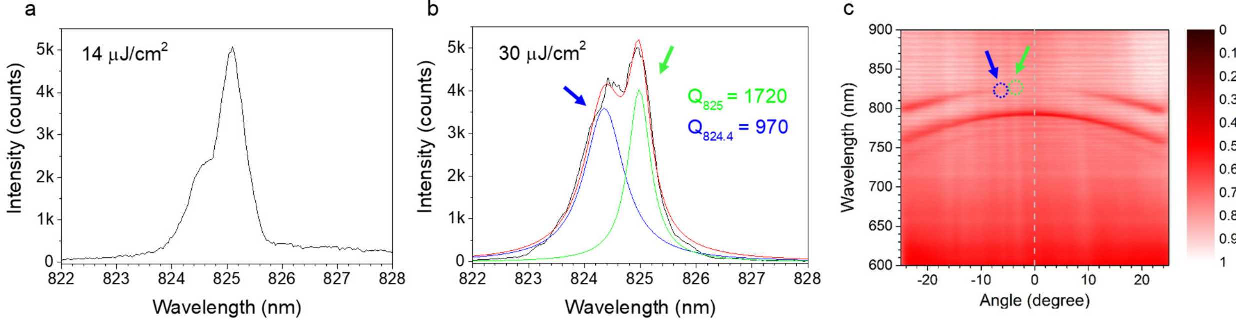

Supplementary Fig.8. Analysis of higher mode lasing at high pumping fluence. a, Emission spectrum at lower pumping fluence (14 μJ/cm^2) showing the fundamental peak at 825 nm dominating the emission. **b**, Emission spectrum at higher pumping fluence (30 μJ/cm^2) showing two-mode emission with comparable strength. Fitting of the emission spectrum reveals the first peak at 824.4 nm having Q = 970 (marked by a blue arrow) and the second peak at 825 nm having Q = 1720 (marked by a green arrow). **c**, Angle resolved transmission spectrum of the sample showing the multi-mode lasing action positions corresponding to panel b. At higher pumping fluence, an additional resonant mode, corresponding to a higher emission angle and shorter wavelength in the resonance band can be co-excited. The primary and secondary modes are depicted with blue and green dashed circles in the angle-resolved transmission spectrum.

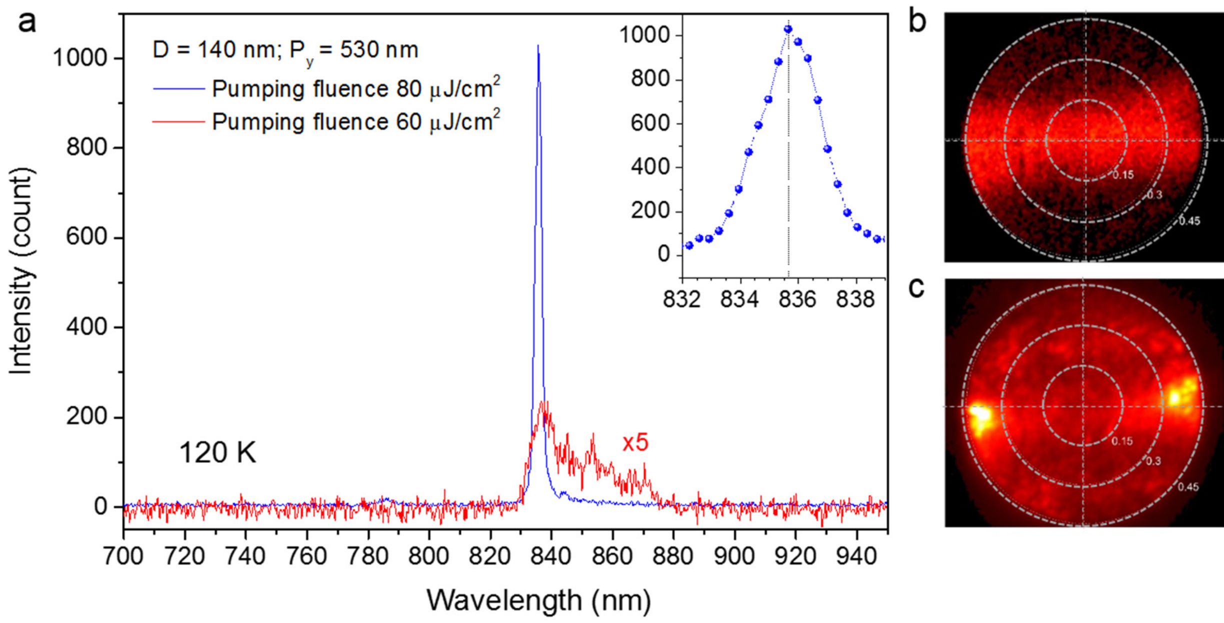

Supplementary Fig.9. Lasing at higher angle in a 2D GaAs array. In these measurements a GaAs array with the following parameters is used: D = 140 nm and P_y = 530 nm which has λ_{BIC} = 850 nm, as shown in Figure 4a in the main text. By changing the temperature to 120 K, for which the PL of GaAs is peaked at 835 nm, we were able to achieve lasing at ~ 836 nm with a lasing angle of ~ 26 degree. **a**, Emission spectra of the GaAs array before (red) and after (blue) the lasing threshold when pumped with a 780 nm femtosecond laser (20 KHz repetition rate, 200 fs pulse width). For lasing experiment at higher temperature than 77 K, we employed a lower repetition rate (*i.e.,* 20 KHz vs 100 KHz at 77 K) to minimize the accumulation of heat leading to sample damage. Inset: zoomed-in lasing peak showing the FWHM of around 2 nm, corresponding to a Q factor of 410. **b** and **c**, Back focal plane images of emission below (b) and above (c) lasing threshold. Above the lasing threshold, two enhanced emission points in the emission plane are clearly seen, corresponding to a lasing angle of around 26 degrees. As discussed in the main text, the lasing happens at the wavelength and angle where a minimum lasing threshold $P_{th}(\lambda)$ ~ $(g(\lambda)\times\Gamma_E(\lambda))^{-1}$ is achieved. In our system, it is possible to tune the gain spectrum of GaAs by changing the device temperature to achieve the minimum threshold, and thus lasing, at a higher angle, as exemplified here.

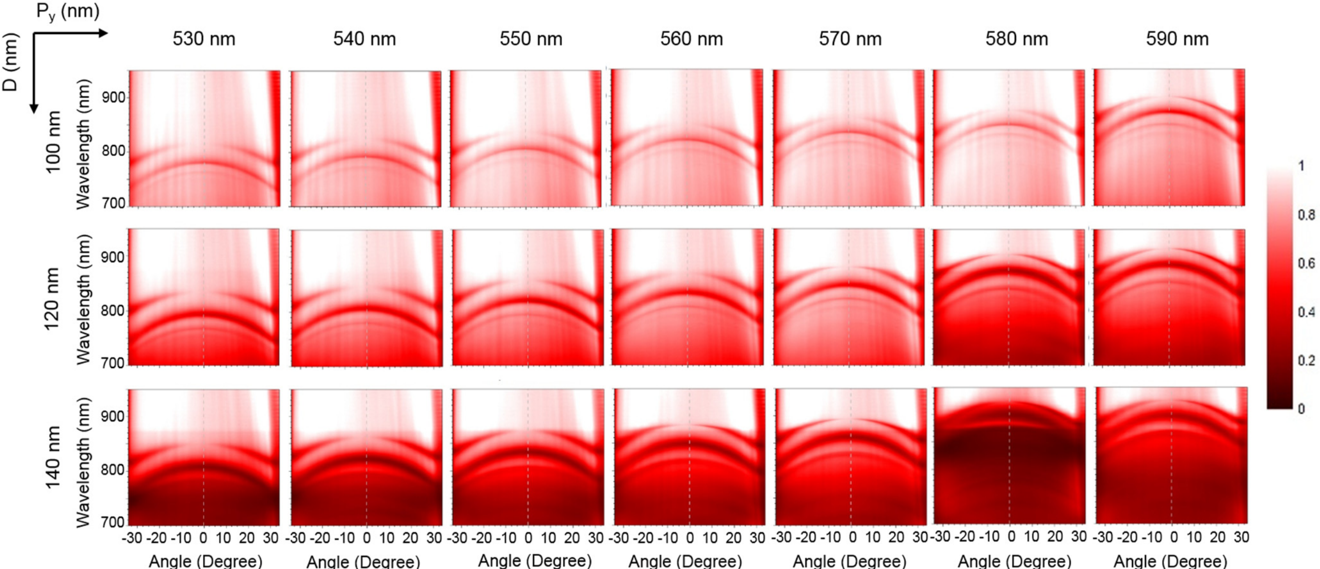

Supplementary Fig.10. Angle resolved transmission measurements for different diffractive array periods and nanopillar diameters (specified in the plot). The geometry of measurements is the same as discussed in Fig.2 in the main text. λ_{BIC} is determined by fitting the transmission dip corresponding to the vertical dipole resonance (*i.e.,* the longest wavelength dip) at 0° angle. The determined λ_{BIC} of the arrays with different periods and particle sizes are summarized in Figure 4a in the main text.

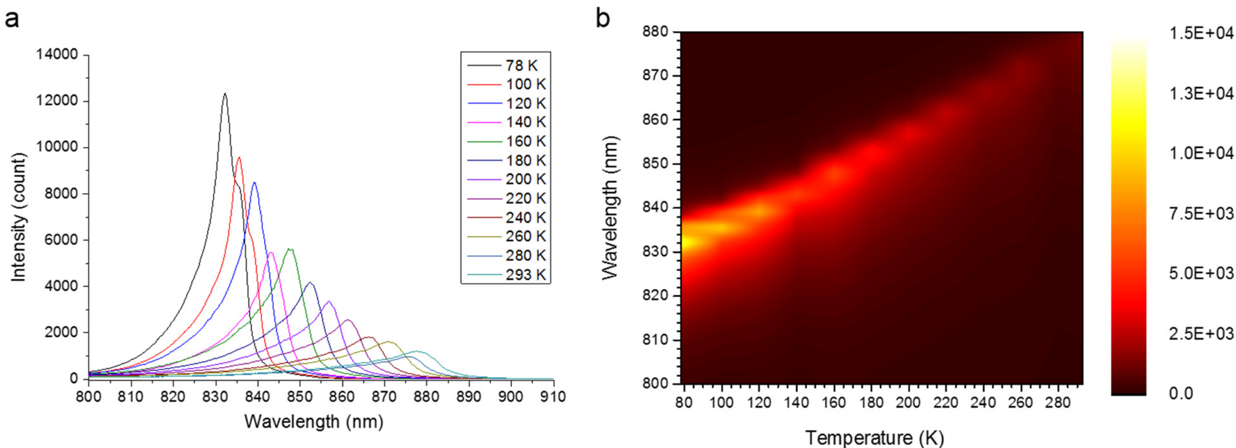

Supplementary Fig.11. Temperature dependent photoluminescence of GaAs films. **a,** PL spectra evolution of a GaAs film at different temperatures. b, Contour plot of the temperature dependent PL (same as in a) is represented to show the emission peak shift and increase of gain (*i.e.*, of the PL intensity) as the

temperature decreases. The PL spectra shown correspond to GaAs films. The PL spectra for nano-sized GaAs pillars are blue-shifted for around 5-10 nm compared to the films, as shown in Figure S5 for the case of PL at 77K. In this case the PL peak of GaAs films happens at ~ 832 nm while for the nanopillar array the PL is peaked at ~ 827 nm. This red-shift may be originated from the heating effect of the GaAs film during laser excitation.

References

1 Lozano, G., Grzela, G., Verschuuren, M. A., Ramezani, M. & Rivas, J. G. Tailor-made directional emission in nanoimprinted plasmonic-based light-emitting devices. *Nanoscale* **6**, 9223 (2014).

2 Yablonovitch, E., Gmitter, T., Harbison, J. P. & Bhat, R. Extreme selectivity in the lift-off of epitaxial GaAs films. *Appl. Phys. Lett.* **51**, 2222-2224, (1987).

3 Yablonovitch, E., Hwang, D. M., Gmitter, T. J., Florez, L. T. & Harbison, J. P. Van der Waals bonding of GaAs epitaxial liftoff films onto arbitrary substrates. *Appl. Phys. Lett.* **56**, 2419-2421, (1990).